

NAT'L INST. OF STAND & TECH R.I.C.



A11105 142043

NIST  
PUBLICATIONS

**NISTIR 6002**

---

# Ultimate Capacity Testing of Laminated Elastomeric Base Isolation Bearings Under Axial Loading

---

Building and Fire Research Laboratory  
National Institute of Standards and Technology  
Gaithersburg, Maryland 20899

QC  
100  
.U56  
NO. 6002  
1997



United States Department of Commerce  
Technology Administration  
National Institute of Standards and Technology



---

---

# Ultimate Capacity Testing of Laminated Elastomeric Base Isolation Bearings Under Axial Loading

---

March 1997

Gregory L. Bradley, Andrew W. Taylor, and Peter C. Chang

Building and Fire Research Laboratory  
National Institute of Standards and Technology  
Gaithersburg, Maryland 20899



U.S. Department of Commerce  
William M. Daley, *Secretary*  
Technology Administration  
Mary L. Good, *Under Secretary for Technology*  
National Institute of Standards and Technology  
Arati A. Prabhakar, *Director*



## ABSTRACT

### Ultimate Capacity Testing of Laminated Elastomeric Base Isolation Bearings Under Axial Loading

NISTIR 5800, "Guidelines for Pre-Qualification, Prototype and Quality Control Testing of Seismic Isolation Systems," defines a Pre-Qualification Test series to determine the Ultimate and Reserve Capacity of an Isolation Unit. In order to improve the current guidelines for these tests, NISTIR 5800 recommends testing full-scale and scale-model base isolation units to failure to determine actual failure loads and to investigate whether similitude relationships apply between full scale and scale model units. Reliable prediction of full-scale bearing ultimate capacities from scale model versions is important since the extremely large load-carrying capacity of most seismic isolation units prevents testing to failure in most existing test facilities. As a step in this direction, this report presents test results to determine ultimate compression under zero lateral load for four laminated elastomeric base isolation bearings. Three of the bearings were nearly geometrically similar (referred to in the report as Type B Bearings) -- full-scale, 1/2-scale, and 1/4-scale models, and were tested to failure. The results of these bearing tests indicate that it may be possible to use scale-models to determine failure loads of full-scale bearings. The stress-strain curves of the Type B Bearings are similar in shape; however, they are not identical. The testing program included only one bearing of each size, and further experiments should be conducted. In a later study, finite element analyses will be conducted to investigate the effect of the geometric dissimilarities on the stress-strain curves of the scale-model bearings. The Type A Bearing was tested first in order to gather experience with the testing procedure and to investigate dependence of bearing response on strain rate. The tests indicate that the bearing response is independent of loading rate over the range of head speeds obtainable with the test machine (maximum head speed of about 0.40 mm/s).

Key Words: building technology; compression testing; earthquake engineering; elastomeric bearings; reserve capacity ; seismic base isolation; testing; ultimate load tests.



## ACKNOWLEDGMENTS

This testing program was supported by the Structures Division, Building and Fire Research Laboratory, National Institute of Standards and Technology, U.S. Department of Commerce through a grant to the University of Maryland (UM).

The authors would like to thank the following individuals without whose assistance these tests could not have been satisfactorily completed: Mr. Eric Anderson for his expert running of the NIST Universal Testing Machine, and Mr. Frank Rankin and Mr. Max Peltz for great help in LVDT calibration and data acquisition.



## TABLE OF CONTENTS

ABSTRACT.....	iii
ACKNOWLEDGMENTS.....	v
TABLE OF CONTENTS.....	vii
LIST OF FIGURES.....	ix
LIST OF TABLES.....	xi
1. INTRODUCTION.....	1
2. DESCRIPTION OF TEST SPECIMENS.....	3
2.1 Dimensions.....	3
2.2 Material Properties.....	8
2.2.1 Rubber Testing.....	8
2.2.1.1 Rubber for Type B Bearings.....	8
2.2.1.2 Rubber for Type A Bearings.....	9
2.2.1.3 Planned tests on rubber.....	10
2.2.2 Steel Testing.....	11
3. DESCRIPTION OF TEST SETUP.....	13
3.1 Test Machine.....	13
3.2 Test Setup.....	15
4. DESCRIPTION OF TEST PROCEDURE.....	19
4.1 Control of Test Machine.....	19
4.2 Dependence on Strain Rate.....	19
4.3 Test Procedure.....	19
5. OBSERVATIONS AND RESULTS OF TESTS.....	21
5.1 Bearing A - First Test.....	21
5.2 Bearing A - Second Test.....	22
5.3 Bearing B1.....	23
5.4 Bearing B2.....	25
5.5 Bearing B3.....	26
5.6 Comparative Plots.....	28

APPENDIX A. FORMAT OF TEST DATA FILES INCLUDED ON FLOPPY

## LIST OF FIGURES

Figure 2.1	Bearing A dimensions .....	5
Figure 2.2	Full-Scale (Bearing B1) dimensions .....	6
Figure 2.3.(a)	1/2-Scale (Bearing B2) dimensions .....	7
Figure 2.3.(b)	1/4-Scale (Bearing B3) dimensions .....	7
Figure 3.1	Test machine .....	14
Figure 3.2	Setup for Bearing A tests .....	16
Figure 3.3	Setup for Bearing B tests .....	17
Figure 4.1	Load-head speed versus load for Bearing A, initial test (2nd cycle) .....	20
Figure 5.1	Load-Displacement plot for Bearing A, first test .....	21
Figure 5.2	Load-Displacement plot for Bearing A, second test .....	22
Figure 5.3	Load-Displacement plot for Bearing B1, full-scale .....	23
Figure 5.4	Head velocity and load during shim failures for Bearing B1, full-scale .....	24
Figure 5.5	Load-Displacement plot for Bearing B2, 1/2-scale .....	25
Figure 5.6	Head velocity and load during shim failures for Bearing B2, 1/2-scale .....	26
Figure 5.7	Load-Displacement plot for Bearing B3, 1/4-scale .....	27
Figure 5.8	Head velocity and load during shim failures, for Bearing B3, 1/4-scale .....	28
Figure 5.9	Comparison of stress-strain curves for all bearings .....	29
Figure 5.10	Comparison of adjusted stress-strain curves for Type B Bearings .....	30



## LIST OF TABLES

Table 2.1	Bearing dimensions.....	3
Table 2.2	Type B Bearings - rubber batches.....	8
Table 2.3	ASTM test results for elastomers.....	9
Table 6.1	Test results summary .....	31

LIST OF TABLES

Table 1	Mean values of the variables
Table 2	Least squares means of the variables
Table 3	Least squares means of the variables
Table 4	Least squares means of the variables

## 1. INTRODUCTION

Seismic base isolation is one of the most promising concepts in seismic resistant construction to come of age in this century. In an effort to facilitate the use of this technology, the National Institute of Standards and Technology (NIST) has published Guidelines for Pre-Qualification, Prototype and Quality Control Testing of Seismic Isolation Systems (NISTIR 5800).

A seismic Isolation System is defined as the collection of Isolation Units, Isolation Components and all other structural elements that transfer force between the foundation/substructure and the superstructure. The Isolation System provides the lateral flexibility and damping necessary for effective isolation, and the high initial stiffness required to resist wind loads. An Isolation Unit is defined as a device that provides all the necessary characteristics in an integral device; an Isolation Component is defined as a device that provides some of the necessary characteristics (e.g. flexibility or damping) in a single device.

Pre-Qualification tests are conducted in order to establish the fundamental properties and characteristics of the isolation system, and need not be related to a specific construction project. The Pre-Qualification Test series includes tests to determine the Ultimate and Reserve Capacity of an Isolation Unit (NISTIR 5800, Section 5.4).

In Section 8.2 of NISTIR 5800, it is noted that further research is needed to better understand the ultimate capacity of seismic isolation devices. Quoting from that section:

Very few Isolation Units and Components have been tested to complete failure, particularly full scale specimens. One reason for this is the extremely large load carrying capacity of most Units and Components and the limitations of existing test facilities. Consequently, the true factor of safety of many of these systems remains an unknown.

Research is needed to investigate the ultimate load carrying capacity of a variety of Isolation Units and Components. The research should include tests on full scale and scale model specimens, and include both vertical and lateral ultimate capacity. Results of the full scale and scale model tests should be correlated so that future tests can be conducted on smaller, less expensive specimens. Failure load models should be refined or developed for these systems and the results verified by experiments. Results of this research should be incorporated into Category II tests described in these guidelines.

Isolation Systems/Units are broadly grouped into three categories: elastomeric, sliding, and hybrid. A common type of elastomeric isolation system is the ordinary laminated bearing, which consists of layers of elastomer and steel bonded under high temperature and pressure to form an integral bearing that is free of joints (elastomer and rubber are used interchangeably throughout this report). The restoring force and damping mechanism are combined in a single device. Sliding systems rely on simple Coulomb friction between two surfaces, and hybrid systems can include aspects of the previous categories, but generally use independent components to provide the restoring force, damping, wind restraint and ultimate restraint.

This report presents the results of testing to determine ultimate compression under zero lateral load for four steel and rubber ordinary laminated base isolation units, three of which are geometrically similar.

# 1. INTRODUCTION

Scientific past isolation is one of the most important factors in the development of a new scientific discipline. The isolation of a scientific discipline is a process that involves the separation of a scientific discipline from other scientific disciplines. This process is often the result of a combination of factors, including the discovery of new scientific phenomena, the development of new scientific methods, and the influence of social and cultural factors.

A scientific isolation system is a system that is designed to isolate a scientific discipline from other scientific disciplines. This system is often used to study the development of a new scientific discipline. The isolation system is designed to prevent the influence of other scientific disciplines on the development of the new scientific discipline. This is done by creating a controlled environment in which the new scientific discipline can develop without the influence of other scientific disciplines.

The purpose of this study is to investigate the factors that influence the development of a new scientific discipline. This study will focus on the role of scientific isolation in the development of a new scientific discipline. The study will also investigate the factors that influence the development of a new scientific discipline, including the discovery of new scientific phenomena, the development of new scientific methods, and the influence of social and cultural factors.

1.1. Isolation  
1.2. Factors

## 2. DESCRIPTION OF TEST SPECIMENS

### 2.1 Dimensions

Specimen B1 is a full scale (or prototype) elastomeric bearing. Specimens B2 and B3 are respectively 1/2 scale and 1/4 scale versions of Specimen B1. These specimens were produced by the same manufacturer with the goal of minimizing any differences in material properties between specimens. Specimen A is not geometrically similar to Specimens B1, B2, and B3, and was manufactured by a different company. All specimens were fabricated using materials and fabrication procedures typical of those used in the manufacture of commercial isolators. Table 2.1 lists important dimensions of each bearing, and Figures 2.1 through 2.3.(b), following the table, are dimensioned drawings of Bearings A, B1, B2, and B3, respectively

Specimen B1 is meant to represent a realistic base isolation bearing, but was not designed for a specific application. It was sized to have a slightly lower capacity than a typical full scale isolator in order to ensure failure in the testing facilities available at NIST.

Even though strict geometric similarity was desired, for various reasons strict geometric similarity was not met in the Type B bearings.

- Layer Thicknesses – For geometric similarity to hold, each shim and rubber layer in Bearing B1 must be twice as thick as Bearing B2 and four times as thick as Bearing B3. Due to a manufacturing error the shims for Bearing B1 are less than twice the thickness of the shims for Bearing B2. Geometric similarity is maintained in shim thickness between Bearings B2 and B3, and between all Type B bearings with respect to rubber thickness.
- Bearing Diameters – The outer diameters of Bearings B1, B2 and B3 could not be made geometrically similar because the manufacturer used readily available molds. The outer diameters of the bonded areas, which correspond to the shim diameters, are geometrically similar. Therefore, the cover layers, consisting of the same rubber as used between the shims, and which protect the shims from environmental exposure, are not geometrically similar. Also, the center alignment holes, which are used to facilitate alignment of the bearing components during manufacture, are not similar.

Table 2.1 – Bearing dimensions

	A	B1	B2	B3
Total Height	584	304	167	109
Total Rubber Layer Thickness (mm)	392	<i>191<sup>1</sup></i>	95	48
Total Shim Thickness (mm)	115.6	37.2	<i>21.3</i>	<i>10.7</i>
Thickness: Each End Plate (mm)	38.1	38.1	25.4	25.4

<sup>1</sup> Dimensions in italics are geometrically similar

Table 2.1 (continued) – Bearing dimensions

	A	B1	B2	B3
Rubber Layers				
# of Layers	39	15	15	15
Thickness (mm)	10.1	<i>12.7</i>	<i>6.4</i>	<i>3.2</i>
Shape Factor <sup>2</sup>	24.4	<i>15</i>	<i>15</i>	<i>15</i>
Total Diameter (mm)	1016	800	406	229
Bonded Dia (mm)	991	762	381	191
Cover Layer Thickness (mm)	2 x 12.5	2 x 19	2 x 12.5	2 x 19
Steel Shims				
No. of shims	38	14	14	14
Thickness (gage)	11 gage	12 gage	<i>16 gage</i>	<i>22 gage</i>
Diameter (mm)	991	<i>762</i>	<i>381</i>	<i>191</i>
Center Alignment Hole <sup>3</sup> Diameter (mm)	76.2	50.1	30.1	30.1
End Plate				
Plan Dimensions (mm)	991 mm diameter	876 mm edge length	508 mm edge length	305 mm edge length

<sup>2</sup> Shape factor (S) is defined as the bonded plan area of the bearing (one side only) divided by the area of the edge of a single layer of elastomer ( $S = d/4t$ , where d is the bonded diameter and t is the rubber layer thickness).

<sup>3</sup> Holes are placed in shim plates to facilitate alignment of the bearing components during manufacture.

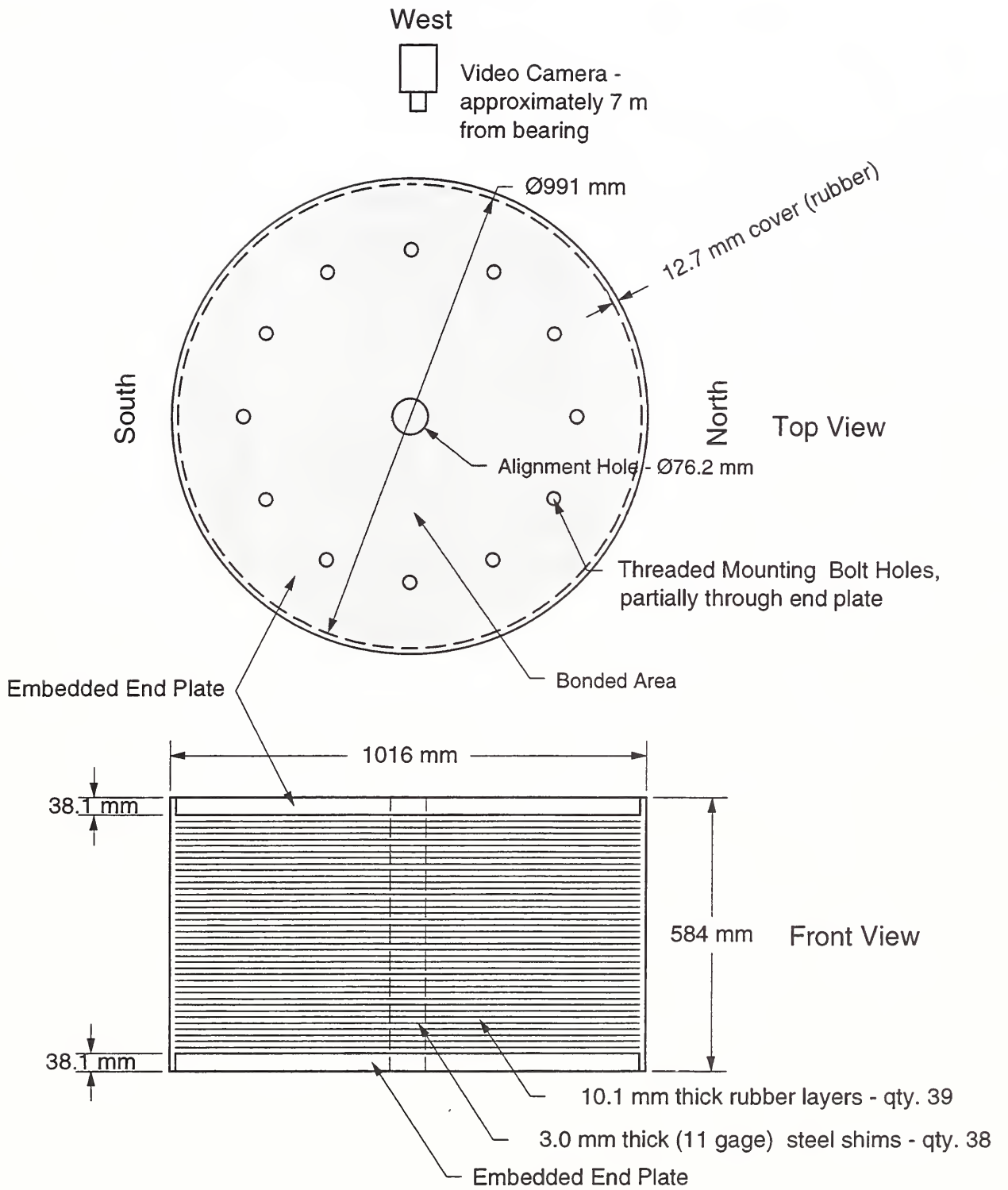


Figure 2.1 - Bearing A dimensions

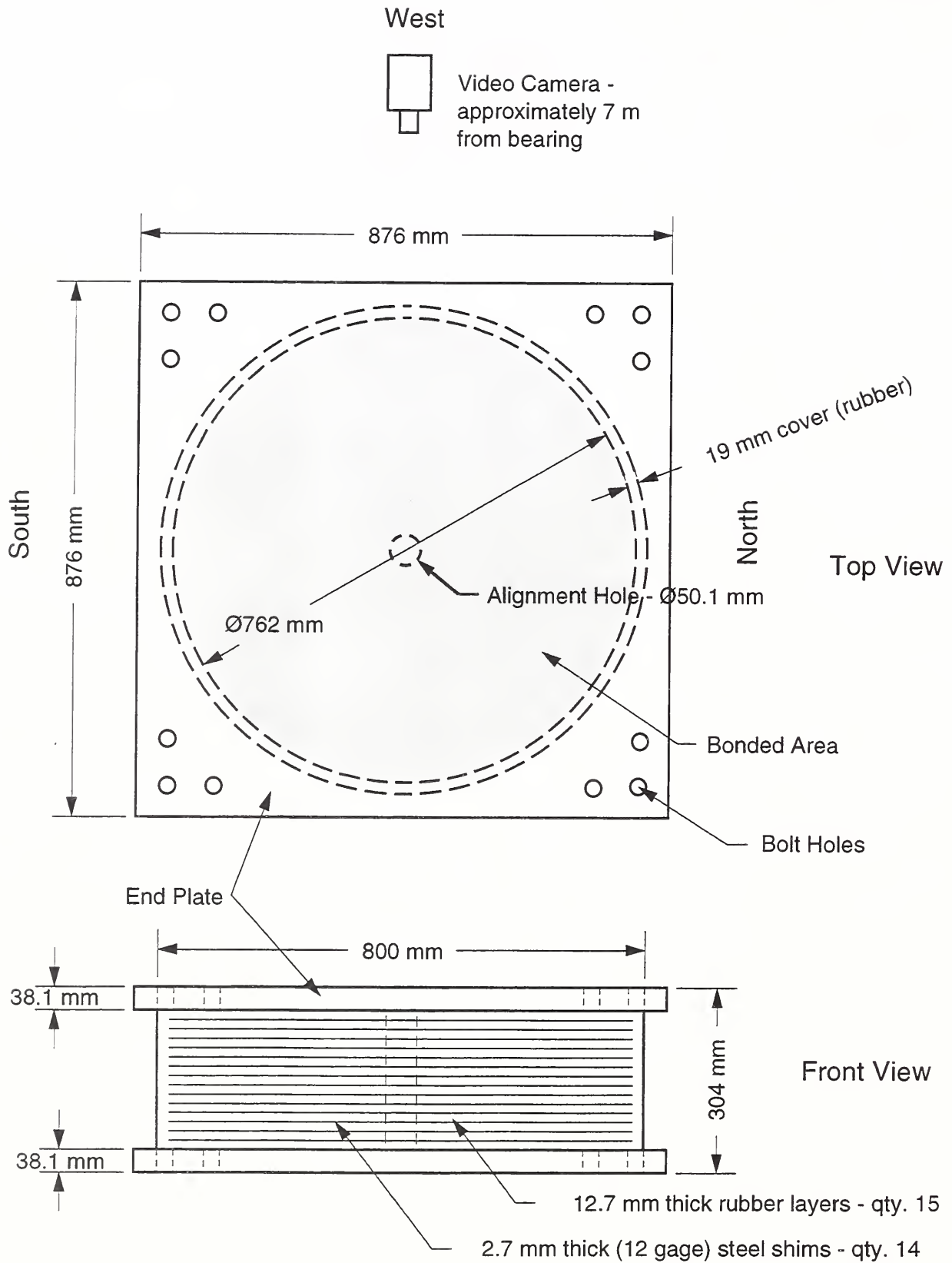
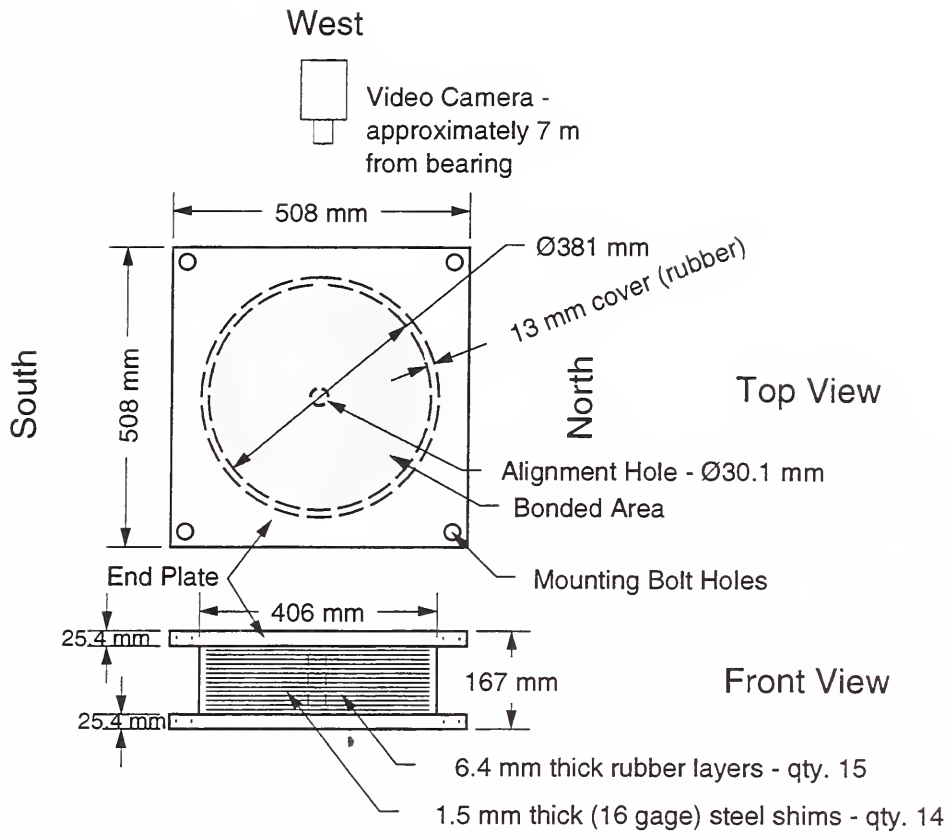
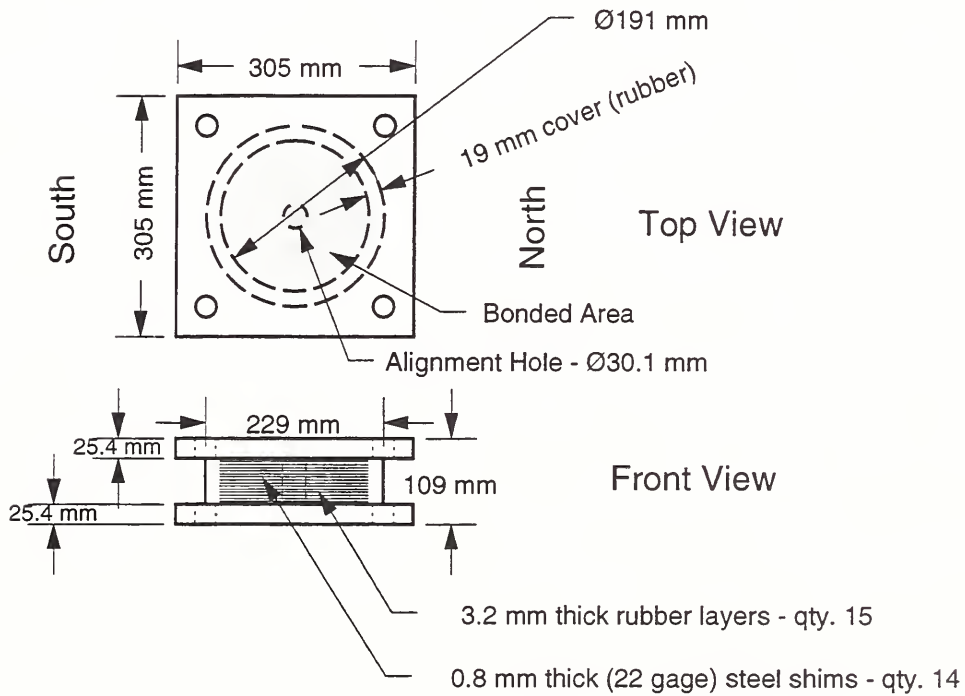


Figure 2.2 - Full-Scale (Bearing B1) dimensions



(a) 1/2-Scale (Bearing B2) dimensions



(b) 1/4-Scale (Bearing B3) dimensions

Figure 2.3 - Bearing dimensions

## 2.2 Material Properties

Shown below are the results of ASTM tests on the rubber compounds. Both bearing types use a high damping natural rubber vulcanizate. Following that is a description of the rubber model to be used in finite element analyses, and which requires uniaxial tensile and compressive test data. These tests have been performed. Finally, there is a discussion of the steel properties and tests performed to fully characterize the steel for finite element analysis.

### 2.2.1 Rubber Testing

#### 2.2.1.1 Rubber for Type B Bearings

All natural rubber used for these bearings came from the same shipment. The natural rubber is mixed with various chemicals, but due to the size of the rubber mixing equipment, three batches were required. Actually, four batches were mixed, but plant quality control rejected the first batch (the rejected batch had been calendared to the wrong thickness). Each batch was blended from identical proportions of identical ingredients. The rubber was vulcanized only after placing the shims and the rubber in alternating layers into a mold.

Two bearings of each size were manufactured; one bearing of each size was tested in this program. The second bearing will be tested to ultimate compression with lateral load applied in a later test program. Table 2.2 shows the batch numbers for each bearing.

Table 2.2 - Type B Bearings - rubber batches

Bearing	Ultimate Compression No Lateral Load	Ultimate Compression Lateral Load Applied (Future Test Program)
B1	Batch 3	Batch 2
B2	Batch 3	Batch 3
B3	Batch 4	Batch 4

As noted above, Batch 1 was rejected by plant quality control. However, for ASTM testing, four of the six tests were conducted using specimens made from a composite batch, which consisted of equal quantities from each of the four batches. The results of ASTM testing are shown in Table 2.3.

### 2.2.1.2 Rubber for Type A Bearings

Test results of the rubber used in the particular bearing tested were not available. The manufacturer, however, reported test results for elastomers with the same chemical composition. These results are shown in Table 2.3.

Table 2.3 - ASTM test results for elastomers

	Shear Modulus [1] ASTM D 4014 Annex A1	Tensile Strength [2] ASTM D 412 Method A	Ultimate Elongation [2] ASTM D 412 Method A	Compression Set [3] ASTM D 395 Method B
Composite Batch	128 psi	2406 psi	621%	20.75%
Batch 1	N/A <sup>4</sup>	2425 psi	597%	N/A
Batch 2	N/A	2537 psi	608%	N/A
Batch 3	N/A	2491 psi	613%	N/A
Batch 4	N/A	2589 psi	664%	N/A
Bearing A elastomer	173 psi	2827 – 2891psi	529% – 579%	N/A

	Shore A Hardness [4] ASTM D 2240	Peel Strength [5] ASTM D 429 Method B	Ozone Resistance [6] ASTM D 1149 <sup>5</sup>
Composite Batch	65	89 lb/in. 100% rubber tear	No cracks at magnification 7X
Batch 1	64	N/A	N/A
Batch 2	65	N/A	N/A
Batch 3	65	N/A	N/A
Batch 4	65	N/A	N/A
Bearing A elastomer	63 - 65	81 - 93 lb/in	N/A

<sup>4</sup> N/A denotes that tests were not performed.

<sup>5</sup> The ozone concentration was 50 parts per hundred million (50pphm). The specimens were stretched to 20% strain, and placed for 100 hours at a temperature of 100° F.

### 2.2.1.3 Additional tests on rubber

Uniaxial compressive and tensile tests have been performed. The nominal stress-strain results are being used to conduct finite element analyses with the finite element code ABAQUS<sup>6</sup> [7]. The basic assumptions for modeling rubbers that ABAQUS uses are

- (1) The material behavior is elastic;
- (2) The material is isotropic, and
- (3) The material is approximately incompressible.

The first two assumptions allow the strain energy potential to be defined in terms of the strain invariants, i.e.  $U = U(I_1, I_2, J)$ , where  $J$  is the volume change. Using assumption (3), approximate incompressibility,  $J \cong 1$ , so  $U = U(I_1, I_2)$ . The ABAQUS code utilizes invariants that separate the deviatoric and volumetric effects. The portion of the deformation gradient  $\mathbf{F}$  that is due to deviatoric effects is denoted  $\bar{\mathbf{F}}$ , and is defined by  $\bar{\mathbf{F}} = J^{-1/3}\mathbf{F}$ . From this,  $\bar{I}_1 = tr(\bar{\mathbf{B}}) = tr(\bar{\mathbf{F}} \cdot \bar{\mathbf{F}}^T)$ <sup>7</sup> and  $\bar{I}_2 = \frac{1}{2}(\bar{I}_1^2 - tr(\bar{\mathbf{B}} \cdot \bar{\mathbf{B}}))$ .

ABAQUS provides two forms of the strain energy function for solid rubber:

- (1) The polynomial form

$$U = \sum_{i+j=1}^N C_{ij} (\bar{I}_1 - 3)^i (\bar{I}_2 - 3)^j + \sum_{i=1}^N \frac{1}{D_i} (J_{el} - 1)^{2i}$$

and

- (2) The Ogden form

$$U = \sum_{i+j=1}^N \frac{2u_i}{\alpha_i^2} (\bar{\lambda}_1^{\alpha_i} + \bar{\lambda}_2^{\alpha_i} + \bar{\lambda}_3^{\alpha_i} - 3) + \sum_{i=1}^N \frac{1}{D_i} (J_{el} - 1)^{2i}$$

In each case, the first summation is the contribution due to deviatoric effects and the second summation is the contribution due to volumetric effects. The subscript “*el*” to the third strain invariant  $J$  refers to the elastic portion of the volume change. For an incompressible material, the second summation in each case is zero. The coefficients  $C_{ij}$ ,  $u_i$  and  $\alpha_i$  are found by ABAQUS using a least-squares curvefit on the experimental nominal stress-strain data.

In general, the results from the Ogden strain energy potential are more accurate than the polynomial form; however, both methods will be run and compared.

---

<sup>6</sup> ABAQUS is a commercially available finite element software code, and is identified in order to adequately specify the analysis and experimental procedures. In no case does such identification imply recommendation or endorsement by the National Institute of Standards and Technology, nor does it imply that this product is necessarily the best available for the purpose.

<sup>7</sup> Dyadic notation – the product of two second order tensors, yielding a second order tensor. In indicial notation, a contraction on one index.

### 2.2.2 Steel Testing

The type of steel for the shims and end plates for the Type A Bearings is unknown. For the Type B Bearings, the shims were made of ASTM A570 Grade 36 steel, and the end plates were made of ASTM Grade A36 steel. Actual tensile coupons from the millings used in manufacture of the shims were tested.

A ductile material yields at stress levels that are orders of magnitude less than the elastic modulus, due to large inelastic strains. As stated in the ABAQUS manual, the relevant stress and strain measures are true (Cauchy) stress and logarithmic strain, and material data for all these models must be given in these measures. True stress and log strain have been experimentally determined from tensile dog-bone specimens.

To prepare the shims for the bonding process with the rubber, they are sandblasted and then coated with a chemical compound in a process known as chemlocking. Tests were done on smooth coupons, sandblasted coupons, and chemlocked coupons in order to determine if these processes have an important effect on the steel material properties. The chemlocked specimens showed a consistently lower yield stress than either the sandblasted or smooth specimens.

The type of steel used in the construction of the bridge is a key factor in determining its strength and durability. The steel used in the bridge is a high-strength, low-alloy steel, which is known for its excellent mechanical properties and resistance to corrosion. The steel is tested to ensure that it meets the required specifications and standards. The testing process involves a series of mechanical tests, including tensile, compression, and shear tests, to determine the steel's yield strength, ultimate tensile strength, and elongation. The results of these tests are used to verify that the steel is suitable for the intended application and to ensure that the bridge is designed and constructed to meet the required safety and performance criteria.

### **3. DESCRIPTION OF TEST SETUP**

#### **3.1 Test Machine**

The Universal Testing Machine is located in the Large Scale Structural Testing Facility (Building 202) at the National Institute of Standards and Technology. It is managed by the Building and Fire Research Laboratory. The test machine has a maximum capacity in compression of 53.4 MN (12 million pounds). See Figure 3.1. The machine has four large screw columns that rise to approximately 23.8 m above ground. The load head is connected to the four columns, and is positioned by moving it up or down on the screw columns. Once in position, the head is locked in place so that throughout the test the head does not move relative to the screw columns. The screw columns extend to about 7.0 m below ground, where a hydraulic cylinder assembly is located. The cylinder is approximately 2.1 m in diameter and is rigidly connected to the four screw columns. As fluid is pumped into the cylinder, the cylinder is pulled down, which pulls the four columns down simultaneously. This, in turn, moves the load head down, forcing the head against the specimen. The maximum stroke of the machine is 1.5 m.

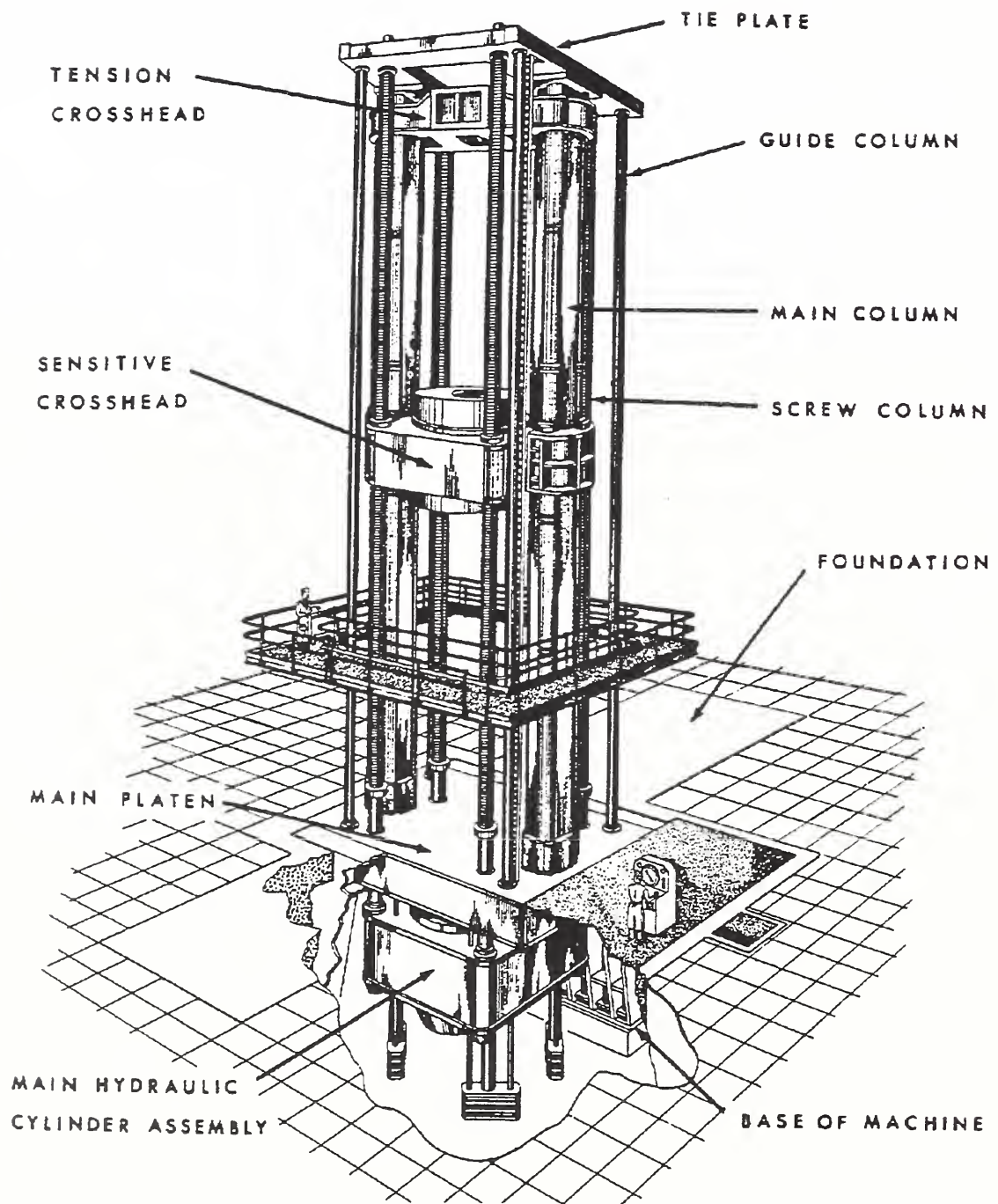


Figure 3.1 - Test machine

### 3.2 Test Setup

For the Bearing A tests, the bearing was placed on two large cylindrical steel plates. These were in turn placed on a reinforced concrete platform designed to withstand greater than 53.4 MN. See Figure 3.2. For the Bearing B tests, the reinforced concrete platform was not used. Instead, a third cylindrical piece of steel was placed on top of the two steel plates used in the Bearing A tests. See Figure 3.3. Also, for each test one smooth steel plate 6.35 mm (1/4 in) thick was placed directly above and below the bearing. This ensured a smooth contact surface, and protected the test machine load head from damage that could result from the irregular surface on the top of the bearings.

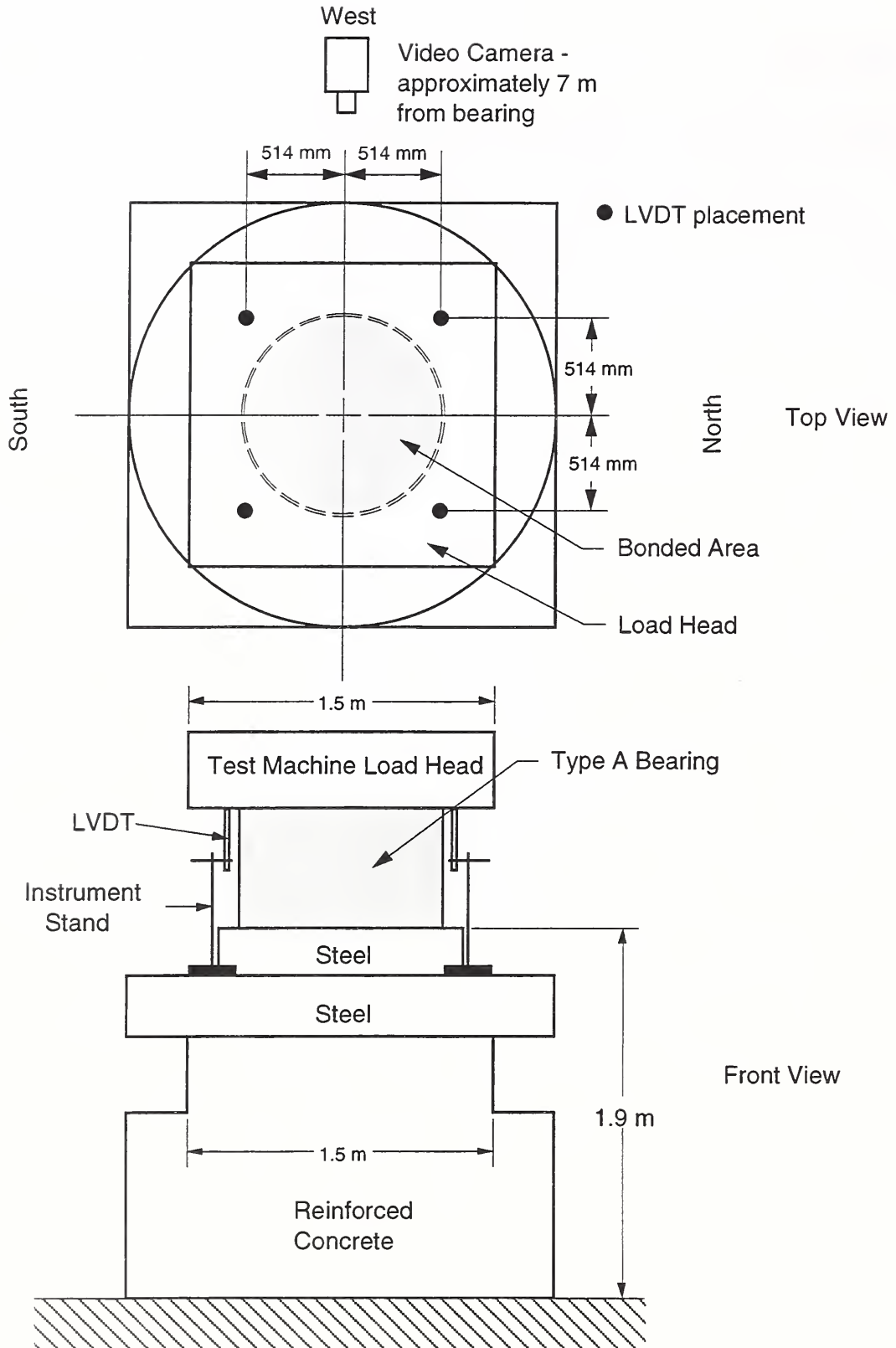


Figure 3.2 - Setup for Bearing A tests

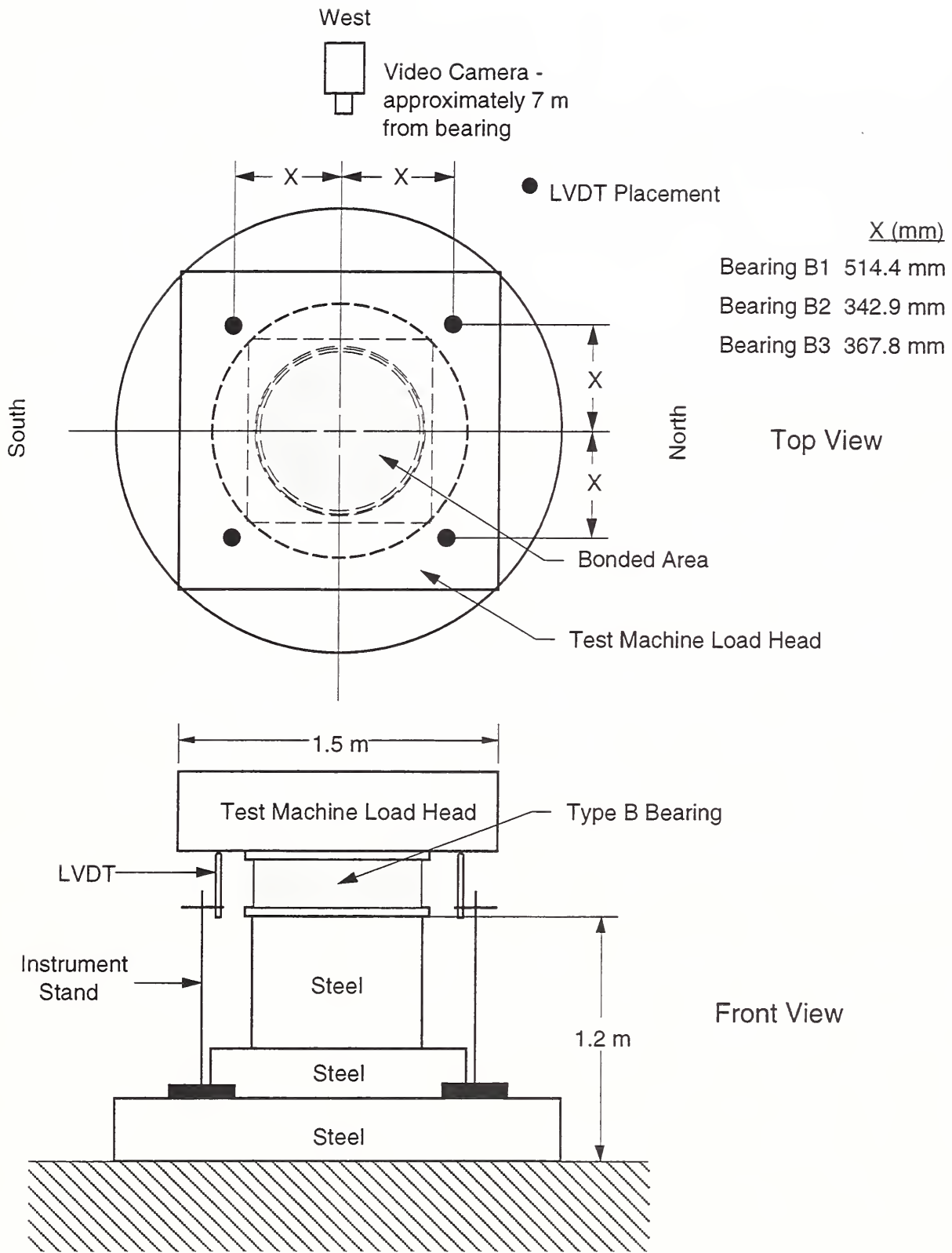


Figure 3.3 - Setup for Bearing B tests

West  
Vibha  
Sri  
Sri



## 4. DESCRIPTION OF TEST PROCEDURE

### 4.1 Control of Test Machine

The test machine is controlled by an open-loop control system. The rate of flow of hydraulic fluid into the test machine cylinder determines the head speed. To control the head displacement, the operator manually adjusts the rate of flow of hydraulic fluid. Load and rate of loading indicated by the movement of the load indicator tells the operator if he is allowing too much or too little fluid to move the head. To maintain a constant head velocity (i.e., a constant rate of flow of hydraulic fluid), the operator must continually increase the valve opening to compensate for a reduced flow rate as the fluid pressure rises. However, even with these manual adjustments, head speed decreases as the load approaches the machine's capacity of 53.4 MN (12 million pounds).

### 4.2 Dependence on Strain Rate

Rubber's stress-strain behavior is a function of strain rate [8]. Based on the response of Bearing A over a range of head speeds, it was concluded that viscoelastic effects can be ignored over the relatively slow range of head speed generated by the test machine. Four sets of three cycles of loading were applied, each to the machine load capacity. The first set was run at the maximum head speed, and the second, third and fourth sets at approximately 50% , 25% , and 10% of the maximum head speed, respectively (the maximum head speed measured in these tests was 0.40 mm/s). As shown in Figure 5.2, the stress-strain curves for each set are virtually identical.

### 4.3 Test Procedure

As described in NISTIR 5800, Section 5.4.1, each bearing was subjected to simple axial compression under zero lateral load. Two tests were run on Bearing A in order to gain experience with test machine control and data acquisition prior to conducting the tests on the geometrically similar bearings B1, B2, and B3.

It is the usual practice in testing elastomeric bearings to mechanically condition the elastomer, since the initial response of an elastomeric specimen is stiffer than the response after even one cycle of loading. The response of the elastomer typically stabilizes after a number of cycles; however, there is no firm guidance on the number of conditioning cycles needed to attain equilibrium. Researchers of bridge elastomeric bearings have used four (4) mechanical conditioning cycles [9]. For dynamic testing, at least six cycles have been recommended by Brown [10]. We decided to use at least six conditioning cycles for this test series. In the first test on Bearing A, seven conditioning cycles to the stress level of 13.79 MPa (2000 psi) compressive stress were applied. In the second test on the Type A Bearing and the subsequent tests on the Type B Bearings, six conditioning cycles were applied to 13.79 MPa compressive stress. Six conditioning cycles were adequate to reach an equilibrium stress-strain curve.

#### Type A Bearing - Initial Test

After mechanical conditioning, five load cycles to the machine capacity of 53.4 MN were applied. The test was run at the maximum speed attainable, which was measured at 0.40 mm/sec. However, Figure 4.1, which shows a plot of head speed versus load for a typical load cycle, clearly shows that maintenance of a constant velocity was not possible. The average speed over this cycle was 0.30 mm./sec, with a standard deviation of 0.09 mm/sec.

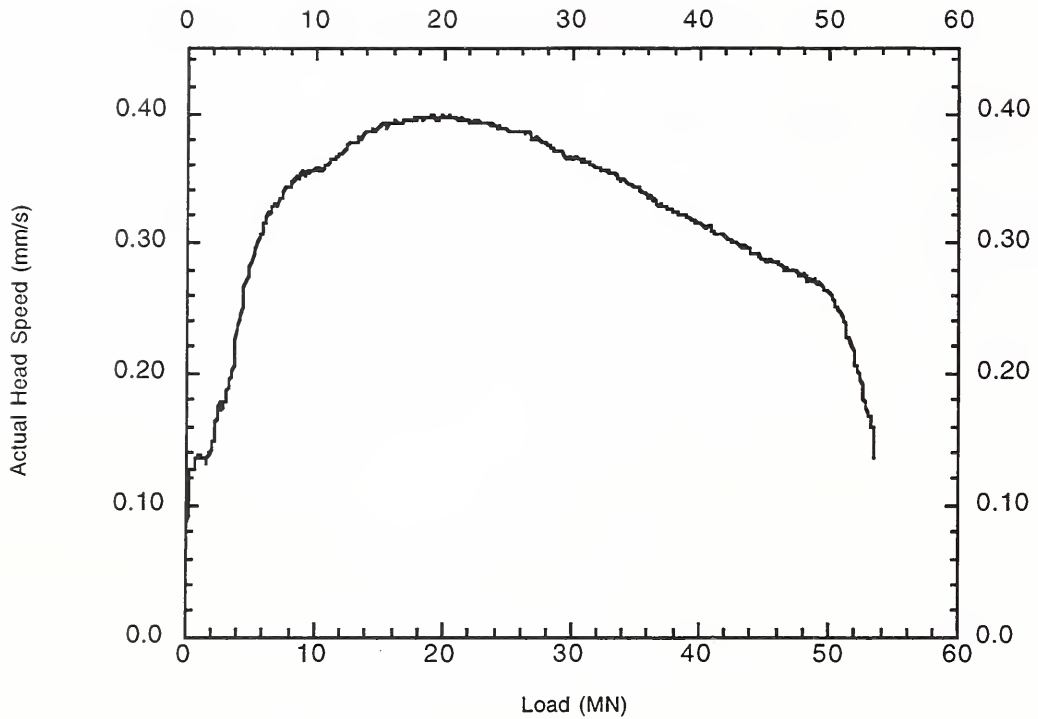


Figure 4.1 - Load-head speed vs load for Bearing A, initial test (2nd cycle)

#### Type A Bearing - Second Test

The second test was run primarily to investigate the influence of strain rate on bearing response. No noticeable difference in bearing response was observed over the range of head speeds attainable by the test machine.

#### Type B Bearings tests

Each of the geometrically similar bearings failed as a result of shim rupture. Accordingly, the loading history consisted of six mechanical conditioning cycles followed by loading to failure. In all cases, load was applied well beyond initial shim failure.

## 5. OBSERVATIONS AND RESULTS OF TESTS

### 5.1 Bearing A - First Test

#### Visual Observations

During the conditioning cycles to 13.79 MPa (2000 psi), bulging of the sides of the bearing was not noticeable. During the load cycles to the machine maximum of 53.4 MN, slight bulging was visible. The middle third of the bearing, as viewed from the West, skewed slightly to the North. There was a slight residual bulge and skew at the conclusion of the test.

#### Load-Displacement Curve

The load-displacement plot (Figure 5.1) shows a change in stiffness at approximately 50 MN compressive force (65 MPa) and 4.2% compressive strain. In each succeeding load cycle, the maximum displacement/strain increased slightly, indicating small increments of permanent deformation. After removal of load, the bearing did not return to its pre-loaded height, thus confirming that inelastic deformation took place during the preceding load cycles. It is reasonable to conclude that the change in slope in the first loading cycle was due to yielding of the steel shims.

Prior to initial yielding, the curve was nearly linear, with a tangent stiffness of 1700 MPa. After the initial yielding, the tangent stiffness dropped by 47% to 900 MPa. The second through fifth load cycles exhibit strain-hardening behavior. Strain-hardening refers to an increasing tangent stiffness as the strain increases, whereas strain-softening refers to a decreasing tangent stiffness as the strain increases. Pure rubber strain-hardens at higher tensile and compressive stresses, and this supports the conclusion that the steel yielded in the initial load cycle to 53.4 MN – the bearing's behavior is dominated more by the rubber than the steel in the second through fifth cycles.

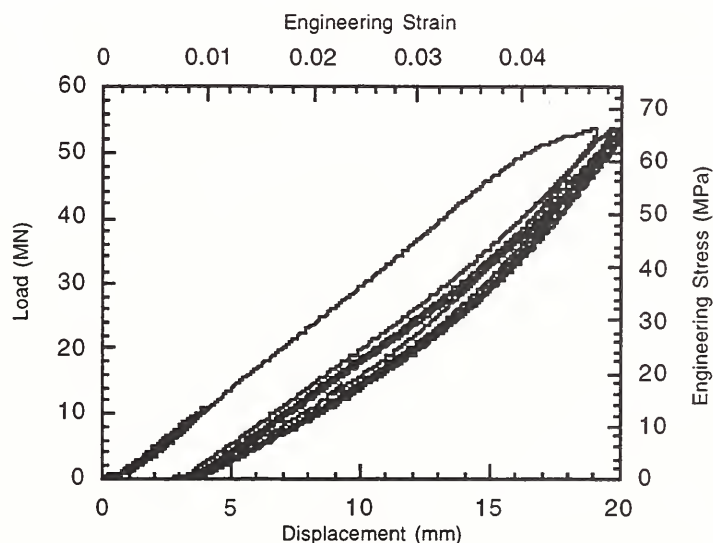


Figure 5.1 - Load-Displacement plot for Bearing A, first test

During the unloading portion of the first cycle, the operator inadvertently reversed the flow of hydraulic fluid, causing a slight increase in load for a moment. This is noticeable in the plot.

## 5.2 Bearing A - Second Test

### Visual Observations

The second test was performed seven days after the first. The slight bulge and skew of the bearing in the northerly direction resulting from the first test was still visible prior to the second test. As in the first test, the bulging and lateral deformation increased when the bearing was loaded.

### Load-Displacement Curve

The general shape of the curves (Figure 5.2) is similar to the curves obtained in the first test after yielding. The vertical compressive strain in the first load cycle of this second test was approximately 4.0% at 53.4 MN, which is about the same as the vertical strain in the second load cycle of the first test (the first cycle after yielding), with the permanent set due to yielding removed. The plot also shows a slight increase in the maximum displacement in each succeeding load cycle, as in the first test.

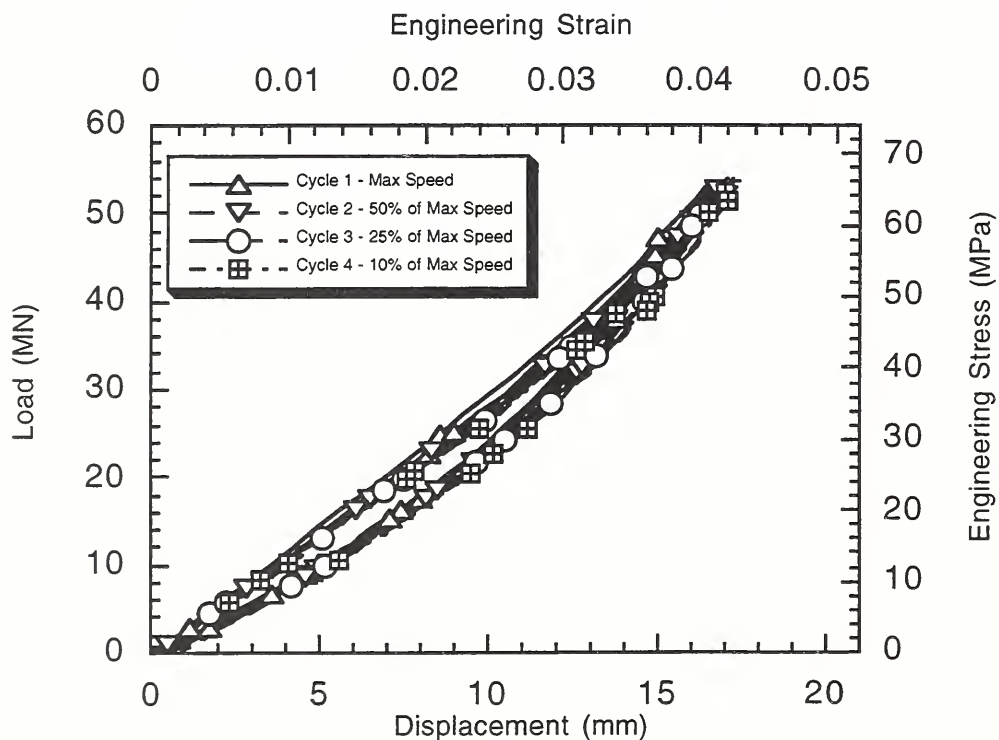


Figure 5.2- Load-Displacement plot for Bearing A, second test

The plot also clearly indicates that the bearing response was virtually identical at head speeds ranging from the maximum head speed down to approximately 10% of the head speed.

Therefore, for the limited range of loading rates examined in this study, bearing response to compressive loading can be considered to be independent of loading rate.

### 5.3 Bearing B1

#### Visual Observations

Bulging was first noticeable at approximately 65 MPa compressive stress and 12% compressive strain, and increased sharply between 80 and 90 MPa. Bulging was greatest at the center, and varied in a parabolic shape from the top to the bottom of the bearing. Bulging appeared to be fairly uniform around the circumference of the bearing. Failure occurred at 90.5 MPa compressive stress and 26.6% compressive strain. Failure was indicated by a loss of strength as displacement continued. This phenomenon was accompanied by an audible rupture emanating from the mid-height of the bearing, followed shortly thereafter by a rapid series of audible ruptures successively further away from the mid-level.

Each audible rupture was followed by a sudden drop in compressive load. Loading was stopped when the load had dropped to less than half its peak value.

#### Load-Displacement Curve

The stress-strain curve (Figure 5.3) shows initial shim yielding at about 42 MPa compressive stress and 6% compressive strain. The shape of the stress-strain curve up to this point indicates strain-hardening behavior, whereas between initial yield and the first shim rupture the bearing strain-softens.

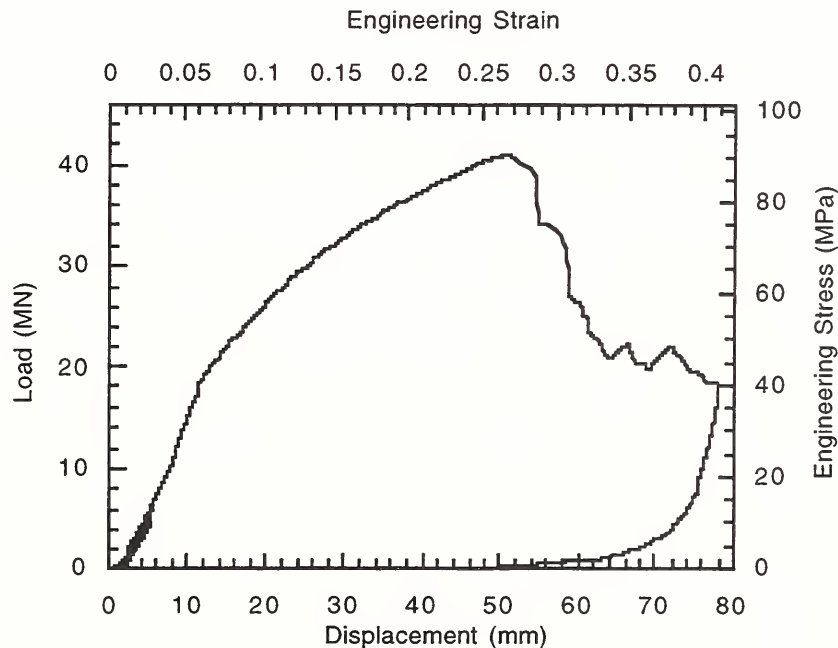


Figure 5.3 - Load-Displacement plot for Bearing B1, full-scale

After the initial shim rupture, displacement was increased at the same rate. As shims failed, the load dropped. Small load recovery occurred between shim ruptures.

### Head Velocity and Load During Failure

Figure 5.4 shows load and head velocity versus time during the failure process. Each velocity peak corresponds to a shim failure. The head velocity at failure was one to two orders of magnitude greater than the head velocity prior to failure. This is consistent with the visual observation that the head movement prior to failure was imperceptible, with downward jumps of the load head observable as shims failed.

After the initial shim failure, resistance decreased rapidly. Five shims ruptured during a period of nine seconds, and the resistance decreased from 40 MN to 21 MN. The bearing then recovered to 22 MN, whereupon another series of ruptures followed. This pattern was repeated once more before the test was terminated.

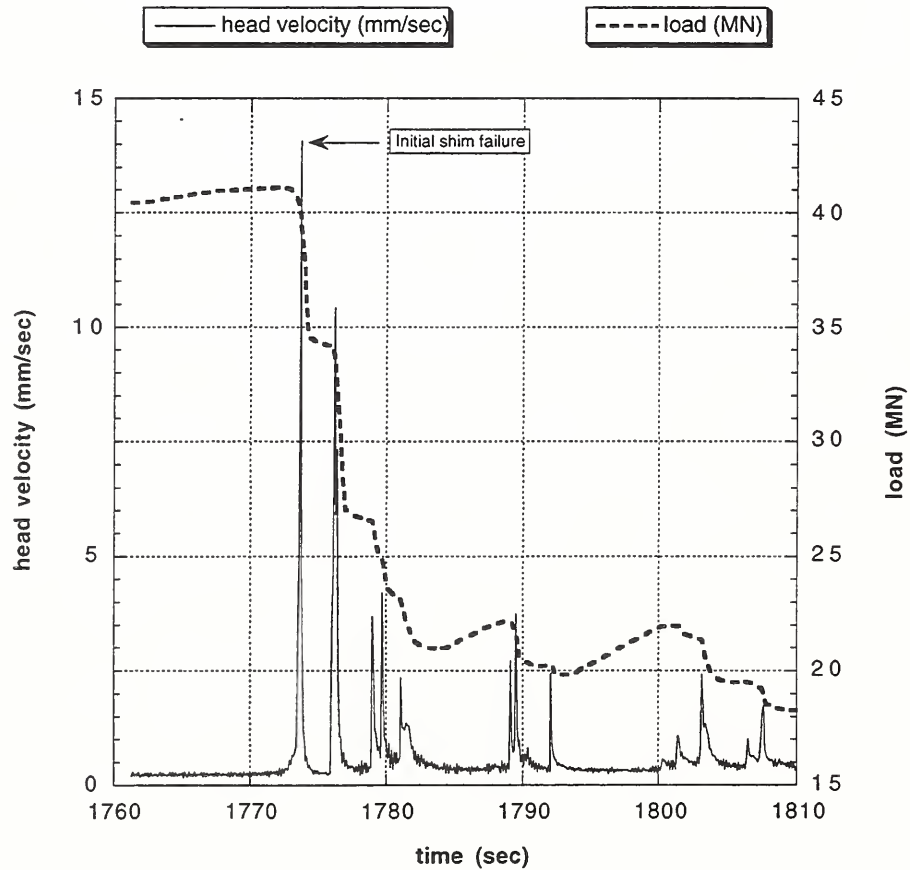


Figure 5.4 - Head velocity and load during shim failures for Bearing B1, full-scale

## 5.4 Bearing B2

### Visual Observations

During loading to failure, bulging became noticeable at about 40 MPa compressive stress and 5.2% compressive strain. The bulging was asymmetric: the bearing bulged significantly on the south and southwest side, and bulged very little on the north and west side. This bulging pattern continued up through failure. Failure occurred at 89.3 MPa compressive stress and 22.8% compressive strain, and was initiated by a shim rupture at or near mid-height, followed by a series of ruptures successively further away from mid-height.

### Load-Displacement Curve

Figure 5.5 shows initial shim yielding at about 45 MPa and about 6% compressive strain. Similar to Bearing B1, the behavior is slightly strain-hardening prior to yield, whereas between initial yield and the first shim rupture the bearing strain-softens.

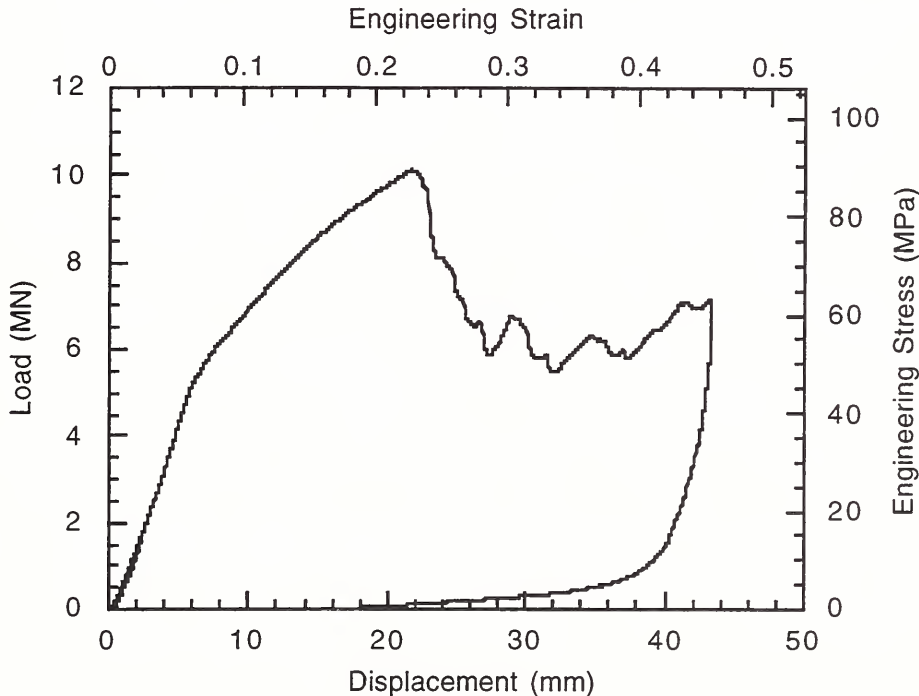


Figure 5.5 - Load-Displacement plot for Bearing B2, 1/2-scale

### Head Velocity and Load During Failure

Figure 5.6 shows load and head velocity versus time during the failure process. Each velocity peak corresponds to a shim failure. The head velocity at failure was one to two orders of magnitude greater than the velocity prior to failure. This is consistent with the visual observation that the head movement prior to failure was imperceptible, with downward jumps of the load head observable as shims failed.

After initial failure, load fell quickly. Over fifteen seconds, there were at least five shim ruptures, and the resistance decreased from 10.7 MN to 5.8 MN. The bearing then recovered to 6.8 MN, whereupon there were another series of ruptures.

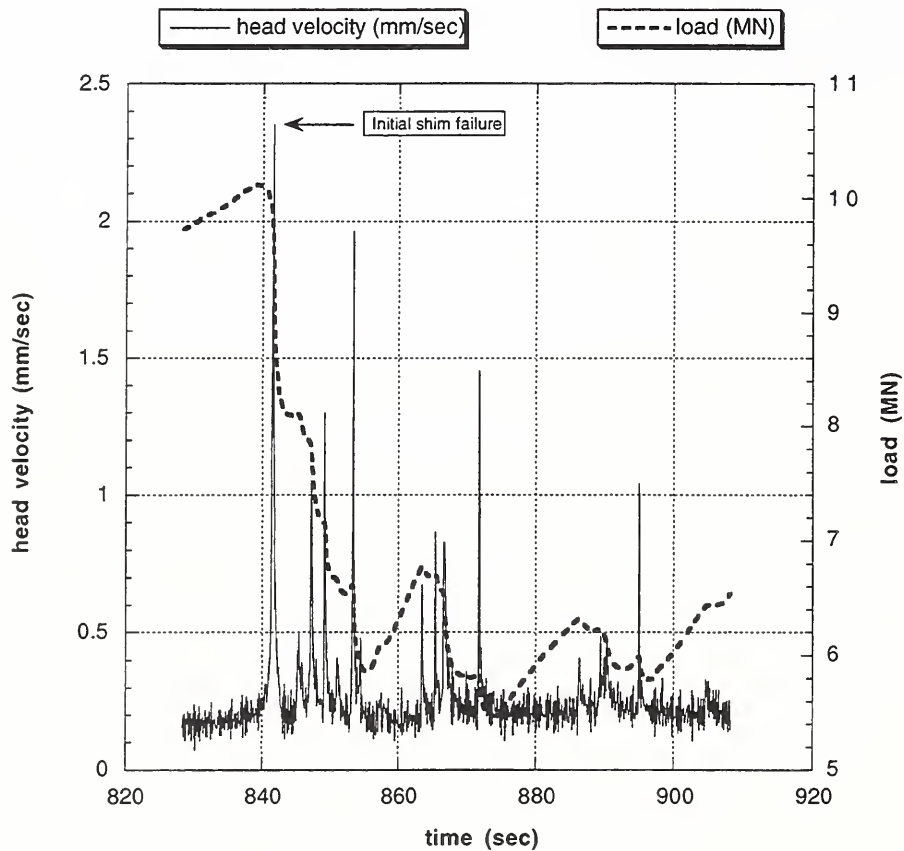


Figure 5.6 - Head velocity and load during shim failures for Bearing B2, 1/2-scale

## 5.5 Bearing B3

### Visual Observations

Bulging was first noticeable at approximately 20 MPa compressive stress and 6.7% compressive strain, and increased steadily to failure, at 99.3 MPa compressive stress and 28.2% compressive strain. Bulging appeared to be uniform around the circumference of the bearing. Bulging was greatest at the mid-height and the shape was parabolic when viewed from the side. Initial shim failure was not audible. It appeared that shim rupture was at or near the mid-height of the bearing, with subsequent failures occurring successively further from mid-height.

In this test, load application was continued considerably beyond failure of all shims. The load carrying capacity eventually increased because after the failure of all shims, the bearing essentially

acted as a single, unbonded layer of elastomer (even bond to the end plates was eventually lost). By the end of the test compressive strains exceeded 75%.

### Load-Displacement Curve

Figure 5.7 shows initial shim yielding at about 52 MPa compressive stress and 7% compressive strain. Similar to Bearings B1 and B2, the behavior is slightly strain-hardening prior to yield, whereas between initial yield and the first shim rupture the bearing strain-softens.

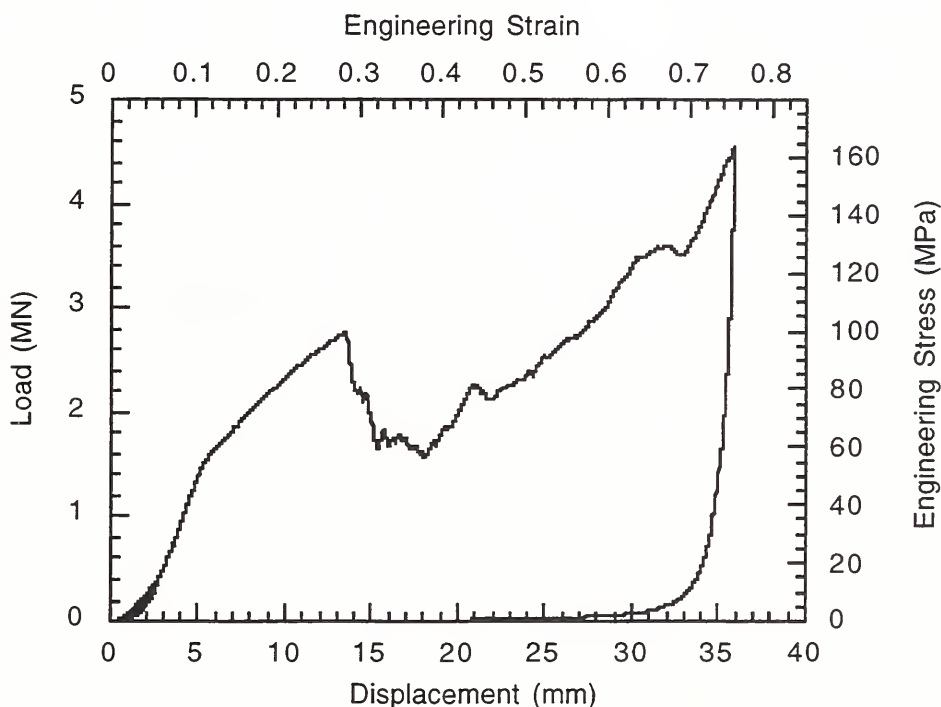


Figure 5.7 - Load-Displacement plot for Bearing B3, 1/4-scale

### Head Velocity and Load During Failure

Figure 5.8 shows load and head velocity versus time during the failure process. Each velocity peak corresponds to a shim failure. The head velocity at failure was one order of magnitude greater than the velocity prior to failure. This is consistent with the visual observation that the head movement prior to failure was imperceptible, with downward jumps of the load head observable as shims failed.

After initial failure, load fell quickly. Over thirty seconds, there were at least five shim ruptures, and the resistance decreased from 2.75 MN to 1.70 MN. The bearing then recovered to 1.85 MN, whereupon there were another series of ruptures.

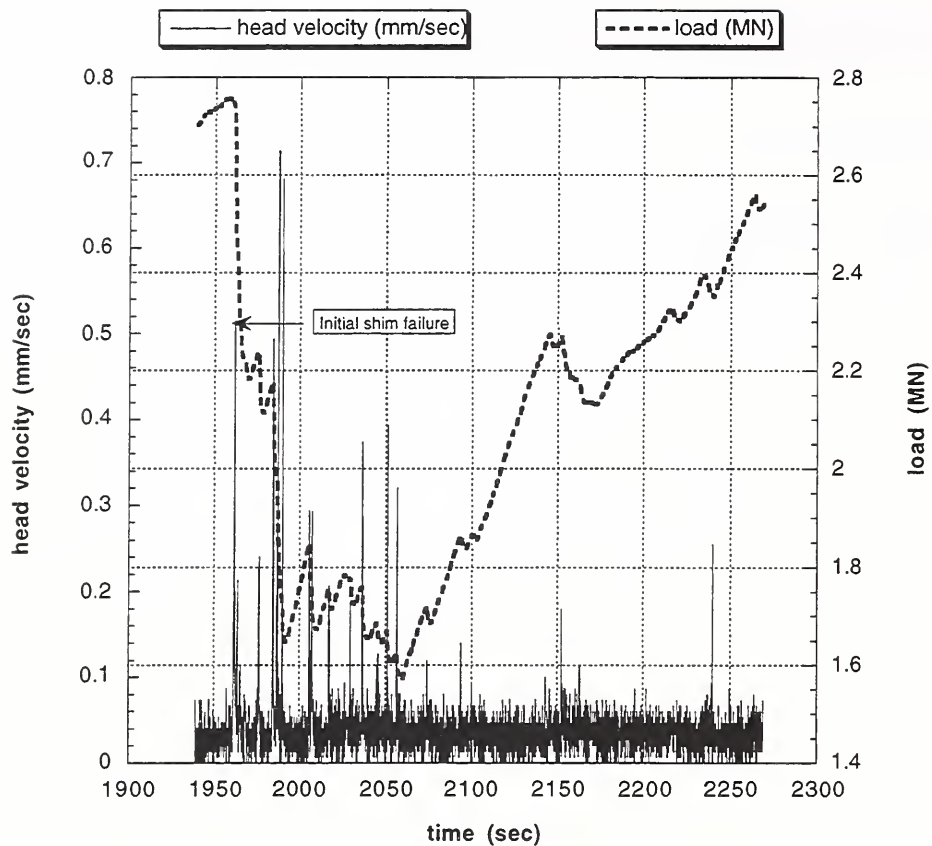


Figure 5.8 - Head velocity and load during shim failures for Bearing B3, 1/4-scale

## 5.6 Comparative Plots

Figure 5.9 shows the stress-strain curves of all specimens on the same plot (the first cycle of loading to 53.4 MN for the Bearing A test is shown). Note the similarity between the three curves for the three Type B Bearings, in spite of the fact that the bearings were not strictly geometrically similar (see Table 1). All curves have similar slopes, except at low stress values. Differences in the initial stiffnesses may be due to misalignment of the load head and end plate.

The approximate tangent stiffness of the Type A Bearing is 1700 MPa just prior to yield. The corresponding stiffness for the Type B Bearings is 930 MPa. Bearing A had a rubber layer shape factor of 24.4, whereas the Type B Bearings had a shape factor of 15. A higher shape factor results in a higher compressive stiffness for the Type A Bearing. This result has been reported by researchers of bridge elastomeric bearings [9], [10], [12].

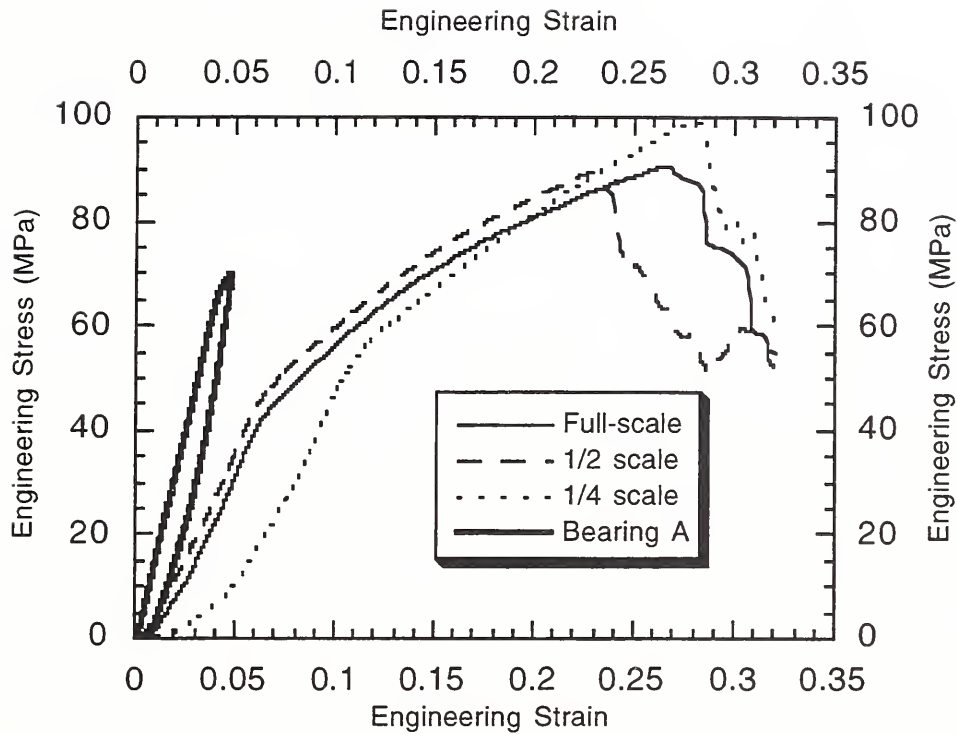


Figure 5.9 - Comparison of stress-strain curves for all bearings

If the lower initial stiffnesses of the full-scale and 1/4 scale models were indeed due to plate and head misalignment, the stress-strain curves can be shifted horizontally. In Figure 5.10, the 1/4 scale stress-strain and full-scale stress-strain curves were shifted to the left by strains of .037 and .005 respectively. This plot clearly shows the nearly identical stiffness prior to initial shim yielding. However, the stress-strain curves, while similar in shape, are clearly not identical. For example, the maximum stress at failure for the full-scale bearing is 90.5 MPa – for the 1/2 scale and 1/4 scale bearings the maximum stresses are 1.3% smaller and 9.6% greater, respectively, than this value. Also, the strain at failure for the full-scale bearing is 0.262, but is 13.0% below this value for the 1/2 scale bearing, and 6.5% below this value for the 1/4 scale bearing. Finally, there is a clear trend toward higher stress and strain at the point of initial yielding as we move from the full-scale bearing down to the 1/4 scale bearing.

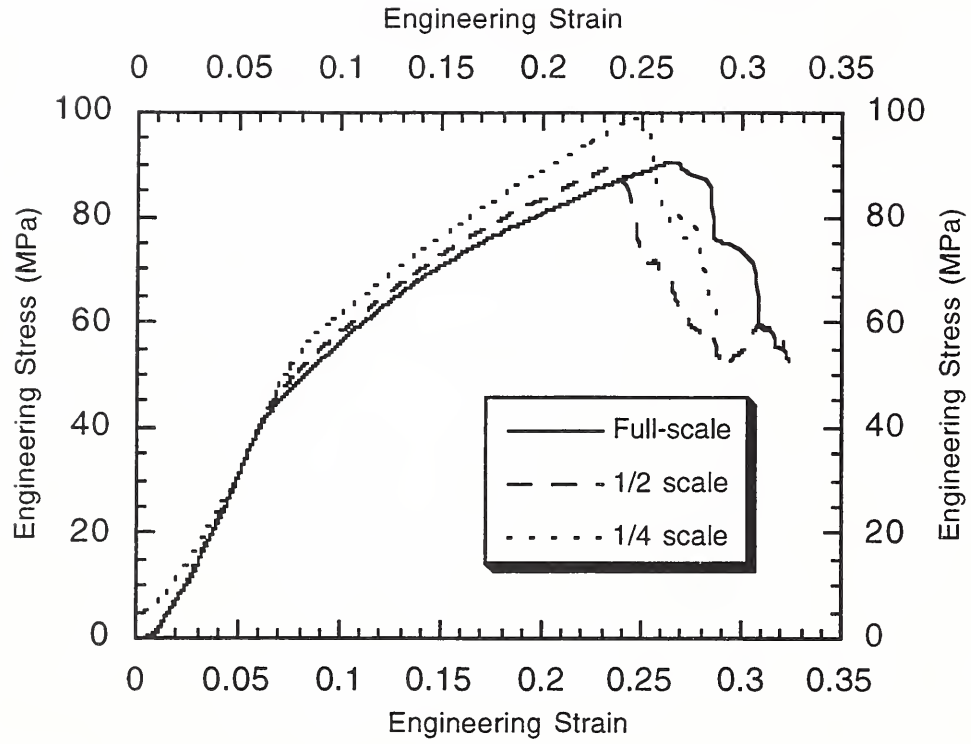


Figure 5.10 - Comparison of adjusted stress-strain curves for Type B Bearings

## 6. SUMMARY AND CONCLUSIONS

The results of these bearing tests indicate that it may be possible to use scale-models to determine failure loads of full-scale bearings. The stress-strain curves of the Type B Bearings are similar in shape; however, they are not identical. It should be remembered that this testing program included only one bearing of each size. Further experiments should be conducted.

In a later study, finite element analyses will be conducted to investigate the effect of the geometric dissimilarities on the stress-strain curves of the scale-model bearings. The finite element model will be calibrated to the full-scale experimental stress-strain curve. Differences between the experimental and analytical stress-strain curves for the scale-model specimens would indicate that the geometric dissimilarity of the bearings does not fully account for the differences in the experimental stress-strain results. Table 6.1 is a summary of the stresses and strains at which initial bulging, initial shim yielding, and failure were recorded for each bearing.

Table 6.1 - Test results summary

Bearing	Initial Bulging		Initial Shim Yielding		Failure	
	Stress (MPa)	Strain	Stress (MPa)	Strain	Stress (MPa)	Strain
A	Not Observed		65	.042	No Rupture Occurred	
B1	65	.12	41.6	.057	90.5	.266
B2	40	.052	44.8	.061	89.3	.228
B3	20	.067	50	.068	99.3	.245

Bearing response should be a function of strain rate, since rubber is a viscoelastic material [2]. However, at the relatively low head speeds of the test machine used in the study, no dependence on strain rate was observed. The maximum speed of the load head was 0.40 mm/s, with an average speed over a full load cycle of 0.30 mm/s and a standard deviation of 0.09 mm/s.

The Type B Bearings show a more nonlinear response than Bearing A prior to initial shim yielding. This is probably due to the lower shape factor of the Type B bearings. The “aggregate” behavior of a bearing with a lower shape factor seems to be more influenced by the rubber. Aggregate is meant in the sense that two distinctly different materials comprise these bearings. In general, rubber strain-hardens, so in a typical stress-strain curve, with strain on the horizontal axis, the shape is concave-upward. Steel, of course, exhibits linear stress-strain behavior prior to yield. The Type B Bearings have a stress-strain curve which shows strain-hardening prior to initial shim yielding, whereas the Type A Bearing, which has less rubber per unit bearing height, has a linear stress-strain curve prior to initial shim yield. Also, there is a stiffer response for bearings with higher shape factors. For Bearing A, with a shape factor of 24.4, the approximate tangent stiffness prior to yield is 1700 MPa. The tangent stiffness reduces to 900 MPa after yield, for a reduction in stiffness of 47%. For The Type B Bearings, with a shape factor of 15, the respective numbers are 930 MPa and 250 MPa, for a reduction in stiffness of 71%.

The Type A Bearing shows initial yielding of the shims at a compressive strain of 4.1%, versus approximately 6.0% for the Type B Bearings. This is to be expected because the two bearing types have different shim thicknesses and shape factors.

## REFERENCES

- 1- ASTM D 4014-89, Standard Specification for Plain and Steel-Laminated Elastomeric Bearings for Bridges, Annex A1, Determination of Shear Modulus
- 2- ASTM D 412-92, Standard Test Methods for Vulcanized Rubber and Thermoplastic Rubbers and Thermoplastic Elastomers - Tension, Test Method A
- 3- ASTM D 395-89 (Reapproved 1994), Standard Test Methods for Rubber Property - Compression Set
- 4- ASTM D 2240-91, Standard Test Method for Rubber Property - Durometer Hardness, Durometer A
- 5- ASTM D 429-81, Standard Test Methods for Rubber Property - Adhesion to Rigid Substrates, Method B
- 6- ASTM D 1149-91, Standard Test Method for Rubber Deterioration - Surface Ozone Cracking in a Chamber
- 7- ABAQUS/Standard Users Manual and ABAQUS Theory Manual (1995), Version 5.5, HKS, Inc.
- 8- Treloar, L.R.G. (1975), The Physics of Rubber Elasticity, 2nd ed., Oxford University Press
- 9- Minor, J.C. and Egen, R.A. (1970), Elastomeric Bearing Research, National Cooperative Highway Research Program Report (NCHRPR) 109
- 10- Brown, R.P. (1986), Physical Testing of Rubber, 2nd ed., Elsevier Applied Science Publishers
- 11- Stanton, J.F. and Roeder, C.W. (1982), Elastomeric Bearings Design, NCHRPR 248
- 12- Roeder, C.W, Stanton, J.F., Taylor, A.W. (1987), Performance of Elastomeric Bearings, NCHRPR 298

## APPENDIX A. FORMAT OF TEST DATA FILES INCLUDED ON FLOPPY DISK

Attached is a PC formatted diskette of the complete load and displacement data files for each test. There are a total of ten files; a load and displacement file for each of the five tests. The files are in ASCII format, and can be imported into many different spreadsheet packages available on personal computers. Each load file contains the load in MN. The displacement files contain the average vertical displacement in mm. In each case, the vertical displacement was adjusted so that zero vertical displacement corresponds to zero load for the first cycle after the conditioning cycles. That is, the residual displacement of the initial conditioning cycles has been subtracted from the displacement data. Time is not included in the files. However, each row of data represents a time step of 0.1 seconds.

In order to fit the data files on one diskette, the files were compressed using the pkzip utility. To decompress each file, at the prompt type `pkunzip "filename"`.

The Bearing A, test 1 files are compressed under A1.ZIP. The decompressed file names are A1\_LOAD and A1\_DISP.

The Bearing A, test 2 files were separately compressed due to their size, and the decompressed file names are A2\_LOAD and A2\_DISP.

The Bearing B tests are all included under B.ZIP. Therefore, decompression will yield six files: Bearing B1 test - B1\_LOAD and B1\_DISP; Bearing B2 test - B2\_LOAD and B2\_DISP; and Bearing B3 test - B3\_LOAD and B3\_DISP.







